Available online at www.sciencedirect.com

SciVerse ScienceDirect

Journal of the European Ceramic Society 33 (2013) 1545–1551

www.elsevier.com/locate/jeurceramsoc

Microstructure–permeability relation of porous β-Si_3N_4 ceramics

Gülsüm Topates [a,*], Lars Mammitzsch [b], Uwe Petasch [b], Joerg Adler [b], Ferhat Kara [a], Hasan Mandal [c]

[a] *Anadolu University, Department of Materials Science and Engineering, Iki Eylul Campus, 26480 Eskisehir, Turkey*
[b] *Fraunhofer Institute for Ceramic Technologies and Systems IKTS, 01277 Dresden, Germany*
[c] *Sabanci University, Material Science and Engineering Programme, 34956 Istanbul, Turkey*

Available online 8 February 2013

Abstract

Porous β-Si_3N_4 ceramics with two distinct structures were produced by using two different Si_3N_4 sources to investigate the relationship between microstructure and permeability. Results showed that regardless of pore amount, size of pore channels, shape-distribution of β-Si_3N_4 grains are more effective on permeability of porous Si_3N_4 ceramics. Higher permeability and lower contribution of inertial forces was obtained by microstructure consists of coarse and equiaxed grains even at lower porosity amount. Calculated Forchheimer number (F_o) and measured the local breadth of a pore also supported the effect of microstructure on permeability.

Keywords: Si_3N_4; Structural applications; Microstructure; Porosity; Permeability

1. Introduction

Combining higher mechanical, chemical and thermal properties with specific grain morphology makes porous Si_3N_4 ceramics one of the favorable materials for filtering applications such as membrane for microfiltration,[1,2] hot gas filter for diesel exhaust systems or coal gasification generation process and catalyst supports.[3–7]

The microstructure of Si_3N_4 ceramics is determined by properties of starting powder, type and amount of oxide additives and sintering conditions. Amount of initial β-Si_3N_4 particles in starting powder is important for final grain size and morphology since these particles are the potential areas for growth of grains. When the amount of β-Si_3N_4 particles is low, grains can find space to grow owing to large interparticle distance. However higher amount of β-Si_3N_4 particles in initial Si_3N_4 source increases the possibility of grain impingement hence more equiaxed and isotropic grains can be produced.[8]

Specific, rod-like grain morphology of β-Si_3N_4 provides excellent mechanical properties.[9–13] Furthermore, β-grains create high surface area so Si_3N_4 becomes important material for filtering applications.[14] The specific surface area of Si_3N_4 with 60–64% porosity was around 1.8 while for SiC whose porosity was 45% and cordierite with 60% porosity were 0.14 and 0.4 m^2/cc respectively.[15] In spite of these favorable properties, random distribution of β-Si_3N_4 grains with small grain width constitutes interlocking structure that has small pore channels. This structure forms a great pressure loss (ΔP) and poor permeability during filtering application.[16]

ΔP and permeability is controlled by some structural parameters such as pore characteristics (pore amount, pore size and distribution, pore shape), specific surface area and tortuosity.[17] Therefore, permeability of porous Si_3N_4 can be improved by tailoring pore characteristics. In previous studies Hayashi et al.[7] and Park et al.[18] used pore formers to enhance permeability behavior. Park et al.[16] showed a novel approach to eliminate the disadvantage of small pore channel size of Si_3N_4 ceramics. They used Si granules (size ranged between 30 and 150 μm) to introduce large pore size in material and were able to increase the permeability of Si_3N_4 to a degree which is close to SiC counterpart.

Relationship between ΔP and ν_s (air velocity) can be used to determine the types of effect on flow regime. Linear relationship between ΔP–ν_s occurs under viscous effects and viscous effects dominate the laminar flow. Quadratic behavior is obtained for ΔP–ν_s when inertial effects prevail and these effects dominate turbulent flow. By using Forchheimer number (F_o) the individual contribution of these effects can be calculated.[19–22]

Anisotropic Si_3N_4 grains with interlocking distribution produce complex pore structure. The complexity of this structure

* Corresponding author. Tel.: +90 222 321 35 50; fax: +90 222 322 29 43.
E-mail address: gtopates@anadolu.edu.tr (G. Topates).

0955-2219/$ – see front matter © 2013 Elsevier Ltd. All rights reserved.
http://dx.doi.org/10.1016/j.jeurceramsoc.2012.12.022

diminishes the distance of flow through the material hence it is important to characterize the porosity profile of the sample. Ziel et al.[23] drew parallel lines with equal distance along the pores and measured the length distribution of the individual line sections and this measured value was called as the local breadth of a pore as it's seen by a particle flowing across the membrane.

This study aims to investigate the possibility of improving permeability of Si_3N_4 by tailoring microstructure. Two types of Si_3N_4 ceramics were produced, their ΔP and permeability were studied. The local breadth of a pore for both ceramics were also plotted to show the effect of pore structure on permeability.

2. Experimental

Materials were prepared by using two different Si_3N_4 powders in this study; α-Si_3N_4 (Silzot H.Q.-Germany, ≥ 80 wt% α-Si_3N_4 and ≤ 1 wt% O, d_{50} = 2.0 μm) and β-Si_3N_4 (Beijing Chanlian Dacheng Trade Co. Ltd., China, ≥ 90 wt% β-Si_3N_4 and ≤ 3 wt% O, d_{50} = 16.6 μm). Series produced from α-Si_3N_4 and β-Si_3N_4 were denoted AC and BC, respectively. $CaCO_3$ (Riedel-de Haen, Germany) was chosen as an additive with amount of 1.44 wt% for both series. Starting powders were milled by planetary mill (Fritsch Pulverisette 5) using deionized water at 100 rpm for 1 h. PEG-1400 (7.5 wt%) was used as binder. Samples with 50 mm diameter and 3 mm thickness were shaped by uniaxial dry pressing at 60 MPa. Binder burnout processes was carried out in a tube furnace at 600 °C for 1 h under air. Pressureless sintering was preferred in a graphite furnace (Thermal Technology LLC) at 1750 °C for 5 h under N_2 atmosphere.

Porosity of samples was measured by Archimedes displacement method. Mercury porosimeter (Micromeritics AutoPore IV 9500) was used to characterize pore size and distribution of samples. Specific surface area of samples was characterized by BET method (Micromeritics ASAP 2020). X-ray diffraction (XRD) (Rigaku Rint-2200) was performed to identify phases by using monochromatic Cu-K_α radiation (λ = 1.5406 Å). Starting powders and fracture surface of the samples were investigated by scanning electron microscopy (SEM) (Zeiss Supra50 VP).

The thickness of the samples was reduced to 500 μm (±100 μm) through a fine cut procedure by using diamond wire saw for ΔP test. The ΔP and permeability were characterized by using air-flow test bench (Topas GmbH). During the test, the samples were sealed by a rubber ring and the differences between inlet and outlet pressure was measured by pressure sensors as illustrated in Fig. 1. Five samples were used for each of series during ΔP test and the maximum flow rate applied was 8 l/min. ΔP test was carried out at 23 °C and under 0.98 atm pressure.

Since both samples showed non-linear flow behavior Darcian and non-Darcian permeability values were calculated by using Darcy–Forchheimer equation for compressible fluids:

$$\frac{P_i^2 - P_o^2}{2P_oL} = \frac{\mu}{k_1}v_S + \frac{\rho}{k_2}v_S^2 \quad (1)$$

where the inlet pressure is (P_i) and outlet is (P_o), thickness of sample is (L), μ is the dynamic viscosity, ρ is the density of ambient air and v_s is fluid velocity. k_1 and k_2 are Darcian and non-Darcian permeability, respectively. The collected data set were fitted according to the least-squares method to a parabolic model of the type: $y = ax + bx^2$, where y was $(P_i^2 - P_o^2)/2PL$ and x was the velocity v_s. The permeability parameters are then calculated from $k_1 = \mu/a$ and $k_2 = \rho/b$.[19–24] The viscosity of air was 1.8×10^{-5} Pa s and its density was 1.17 kg/cm^3.

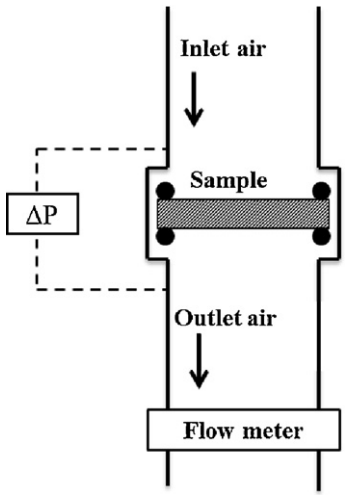

Fig. 1. Schematic description of air-flow test bench.

To observe the microstructural effects and compare to experimental results, k_1 and k_2 were calculated through Ergun's equations:

$$k_1 = \frac{\varepsilon^3 d_p^2}{150(1-\varepsilon)^2} \quad (2)$$

$$k_2 = \frac{\varepsilon^3 d_p}{1.75(1-\varepsilon)} \quad (3)$$

where ε is the volumetric porosity. Based on the previous studies,[24–26] average particle diameter and pore size were used as d_p value. Hence, individual influence of grain and pore characteristics could be predicted. The width of 200 β-Si_3N_4 grains from polished SEM images were measured by image analysis (Image J 1.46R) and averaged.

The materials' flow behaviors were characterized by calculating F_o from Eq. (4). This dimensionless number indicates either viscous or inertial flow regime contribute to ΔP.

$$F_o = \frac{\rho v_s}{\mu}\left(\frac{k_1}{k_2}\right) \quad (4)$$

By using Eqs. (5) and (6), it is possible to calculate the individual contribution of viscous and inertial resistances on the total ΔP.[19,24,27,28]

$$\frac{\Delta P_{viscous}}{\Delta P_{total}} = \frac{1}{1+F_o} \quad (5)$$

$$\frac{\Delta P_{inertial}}{\Delta P_{total}} = \frac{F_o}{1+F_o} \quad (6)$$

To measure the local breadth of a pore, samples used in ΔP–v_s test were mounted by vacuum impregnation and polished. SEM

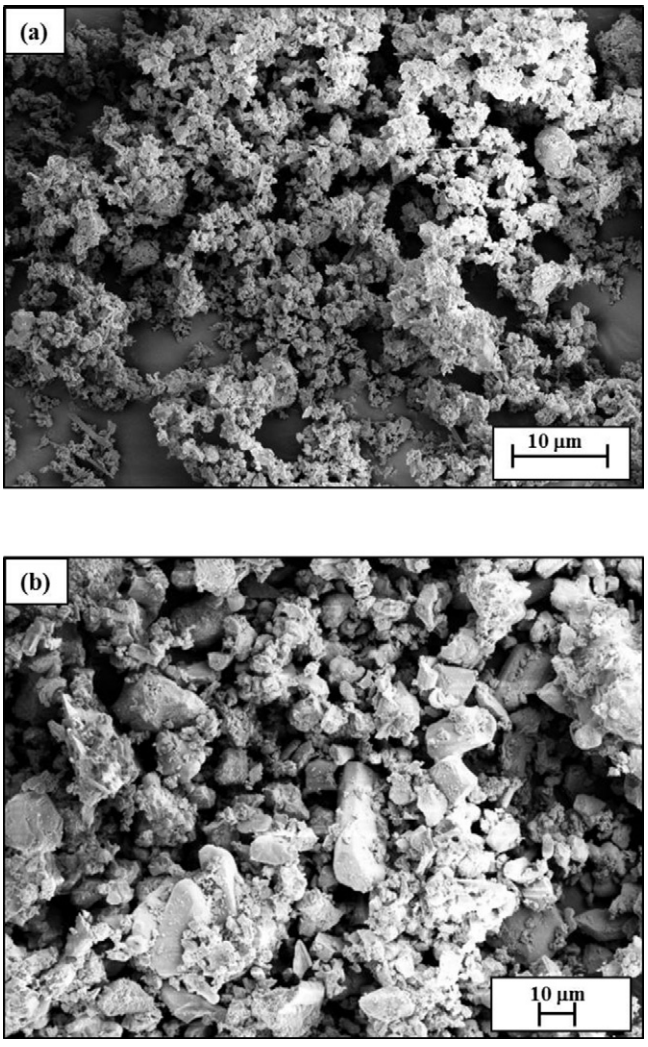

Fig. 2. SEM images of starting powders (a) α-Si_3N_4 and (b) β-Si_3N_4.

images obtained from these polished surfaces were converted binary images. Lines with equal distance were superimposed into these binary images along the flow direction. The length of each line in a single pore was measured and calculated average value was called "the local breadth of a pore". Same procedure was done for 200 pores and distribution of them was plotted.

3. Results and discussion

3.1. Physical properties of samples

SEM images of α-Si_3N_4 and β-Si_3N_4 starting powders were given in Fig. 2a and b, respectively. α-powder consists of large agglomerates whose size is around 10 μm but the primary particle size is about 2 μm. Particle size of β-powder is wider and it consists of particles between 2 and 30 μm.

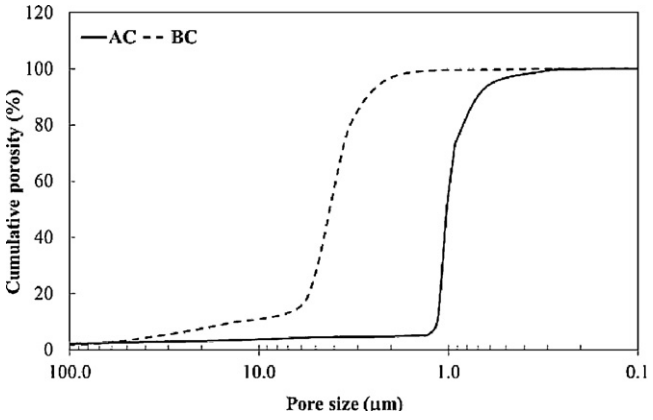

Fig. 3. Cumulative pore size distribution of AC and BC.

CaO was preferred as sintering aid owing to significant contribution on production of high aspect ratio β-Si_3N_4 grains. Physical properties of samples AC and BC were listed in Table 1. Even though using the same amount of sintering additive for both compositions, BC had lower porosity owing to higher oxygen content of starting powder. Rod-like structure of grains in AC has increased its specific surface area by 2.5-fold compare to BC's.

Fig. 3 shows cumulative pore size distribution of samples. While a narrow distribution between 0.4 and 1.5 μm was observed for AC, there is a wider distribution between 2 and 10 μm in BC. d_{50} value of AC was around 1 μm and for BC it was 4 μm.

The XRD analysis, as given in Fig. 4, confirmed that both samples consist of only β-Si_3N_4 phase and that BC has a minor

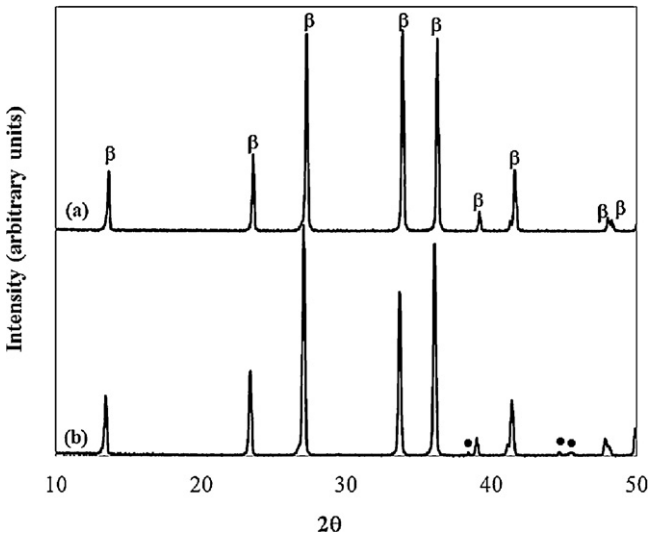

Fig. 4. XRD diffraction pattern of samples (a) AC and (b) BC (β: Si_3N_4, •: secondary phase).

Table 1
Physical properties of AC and BC.

Sample	Bulk density (g/cm^3)	Open porosity (%)	Pore size-d_{50} (μm)	Specific surface area (m^2/g)	Grain diameter (μm)
AC	1.59 (±0.02)	51.5 (±0.7)	1.0	2.5 (±0.11)	1.64 (±0.9)
BC	1.98 (±0.01)	39.1 (±0.1)	4.0	0.9 (±0.03)	14.4 (±6.3)

amount of secondary phase formed by impurities from starting powder.

Fig. 5a and b showed the importance of starting powder type on the development of Si_3N_4 microstructure. Although, β-Si_3N_4 was the major phase in both samples, AC had characteristic, elongated β-Si_3N_4 grains, while grains in BC are in more isotropic nature.

These microstructural differentiations can arise from;

a) Location of precipitation: Phase transformation of Si_3N_4 occurs by dissolution of α-grains into the liquid phase and precipitation as β-grains. Location of precipitation has an important role for the microstructural development. If starting powder has a high amount of α-Si_3N_4, β-grains can precipitate on new β-nuclei formed by local supersaturation accompanying of formation specific, anisotropic β-grains. In the case of a high content of β-Si_3N_4 in the powder, β-grains tend to form by precipitating on already existed β-particles and a coarser and more equiaxed microstructure is obtained.[29,30] Lange[31] used in his study two Si_3N_4 powder; a high α-Si_3N_4 content (85% α) and a high β-Si_3N_4 content (26% α) and the results showed that isotropic grains were produced with β-powder, while the fibrous grain morphology was obtained with α-phase powder. Okamoto et al.[32] showed that the presence of small amount of β-Si_3N_4 in the starting powder, produced coarser and more equiaxed grains by precipitation on pre-existing β grains.

b) Grain impingement effect: Kramer et al.[33,34] showed the influence of number of initial β-particles on grain size and morphology of β-Si_3N_4. Low number increases interparticle distance where grains can find more space to grow without any grain impingement effect. If higher amounts of β-particles exist in the starting powder, the distance is decreased and through the impingement of grains, an equiaxed morphology is obtained.

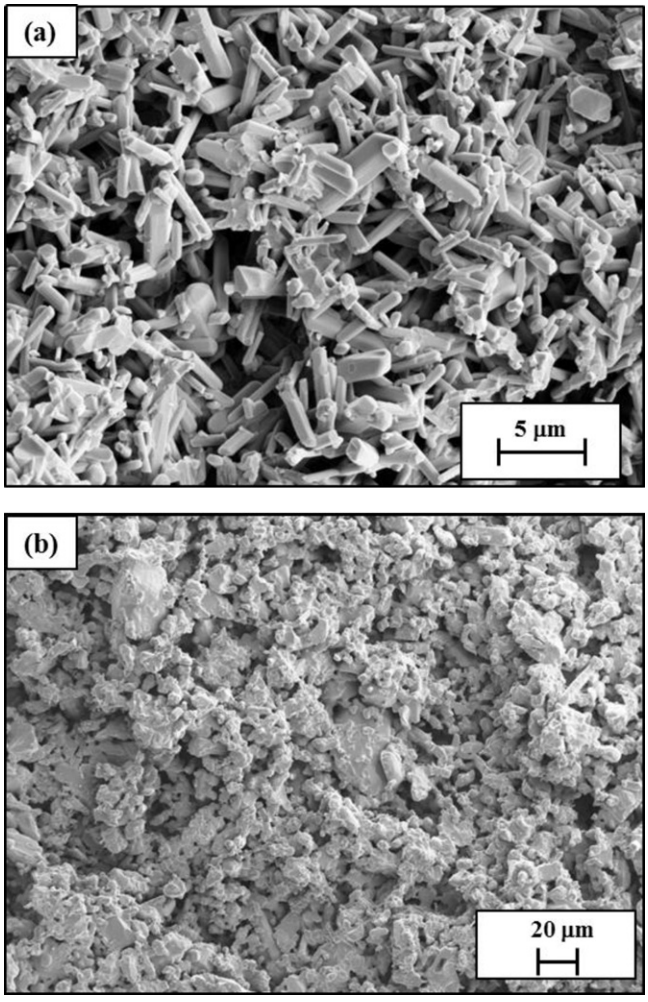

Fig. 5. SEM images from fracture surfaces of porous Si_3N_4 (a) AC and (b) BC.

3.2. Permeability of samples

Fig. 6 displays $(P_i^2 - P_o^2)/2P_oL$ vs. ν_s curves of AC and BC. Since five samples were tested from each of the series, standard deviations were also added to the curves. Samples from AC presented higher deviations than BC. It is clear that AC had more quadratic dependence than BC and at higher ν_s values this dependence also increased.

Even though both series consist of β-Si_3N_4 as a major phase and AC has higher porosity, experimental k_1 and k_2 values from Fig. 7(a) and (b) showed that AC has relatively lower permeability. Experimental k_1 and k_2 values of AC were $7.1 \times 10^{-14}/m^2$ and $6.2 \times 10^{-10}/m$, respectively while that values for BC were $19 \times 10^{-14}/m^2$ and $32 \times 10^{-10}/m$. The elongated and interlocking structure combining with smaller pore channels impeded the regular air flow through the AC regardless of having more voids for flow.

Permeability values calculated by using Eqs. (2) and (3) were included to Fig. 7(a) and (b). Predicted k_1 values from average diameter and pore size showed better agreement with experimental data than k_2. Especially, calculated values of BC were more compatible with experimental results. Microstructure had less anisotropic grains yielded less errors during estimating permeability. For Darcian permeability grain diameter and for non-Darcian permeability pore size gave more reliable estimation.

Previous studies about permeability of porous Si_3N_4 applied different measuring method such as porometer[7,16,18] or custom made test bench,[35] utilized various estimation techniques like Carman-Kozeny[18] hence reliable comparison cannot be done.

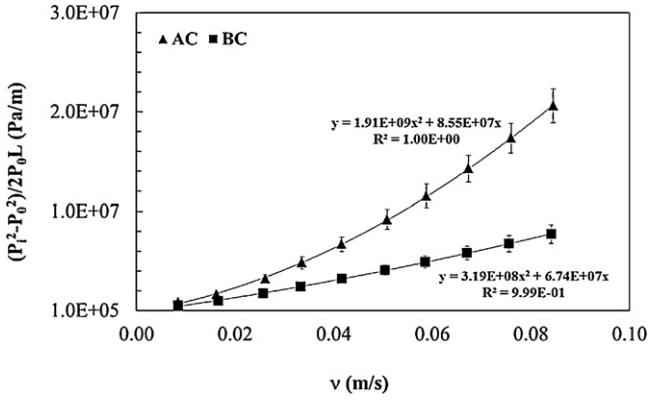

Fig. 6. Experimental permeability data of AC and BC as a function of fluid velocity.

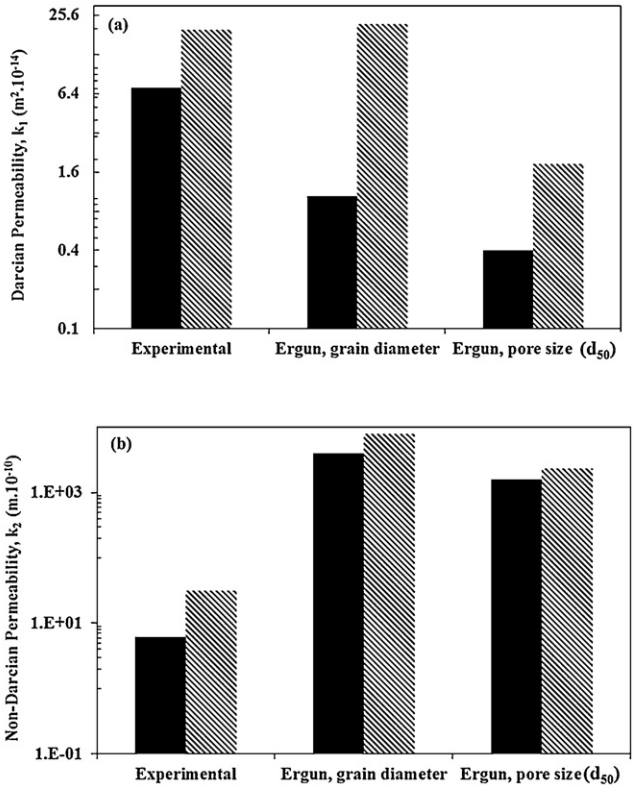

Fig. 7. Experimental and calculated (a) Darcian and (b) non-Darcian permeability values of AC (■) and BC (▨).

3.3. Effect of microstructure on flow regime

As mentioned in the previous section, ΔP of AC performed more quadratic dependence due to increasing effect of inertial regime. To quantify this dependency F_o from Eq. (4) and percentage of contribution of both viscous and inertial effect on total ΔP from Eqs. (5) and (6) were calculated and reported in Table 2 under flow velocity range 0.01–0.1 m/s. AC has higher F_o than for BC. For both samples viscous effect was more dominant. Higher F_o rised the contribution of inertial forces on AC. The value of contribution at the maximum velocity was 39% and 22%, respectively for AC and BC.

Polished, binary and processed SEM images of AC and BC were given between Figs. 8a–c and 9a–c. Gray area represented β-Si_3N_4 grains, bright area was liquid phase formed during sintering and pores were in the black region. When the image was converted to binary image, it consisted of only two regions; black zone represented β-Si_3N_4 grains with liquid phase, while the white area indicated the pores. Lines with equidistance were drawn to binary image as described in experimental procedure.

Table 2
Calculated F_o and contribution of viscous and inertial effect on ΔP (from Eqs. (4)–(6)).

Property	AC	BC
F_o	0.08–0.62	0.03–0.29
$\Delta P_{viscous}/\Delta P_{total}$ = (%)	92.5–61.8	96.9–77.6
$\Delta P_{inertial}/\Delta P_{total}$ = (%)	7.5–39.2	3.4–22.4

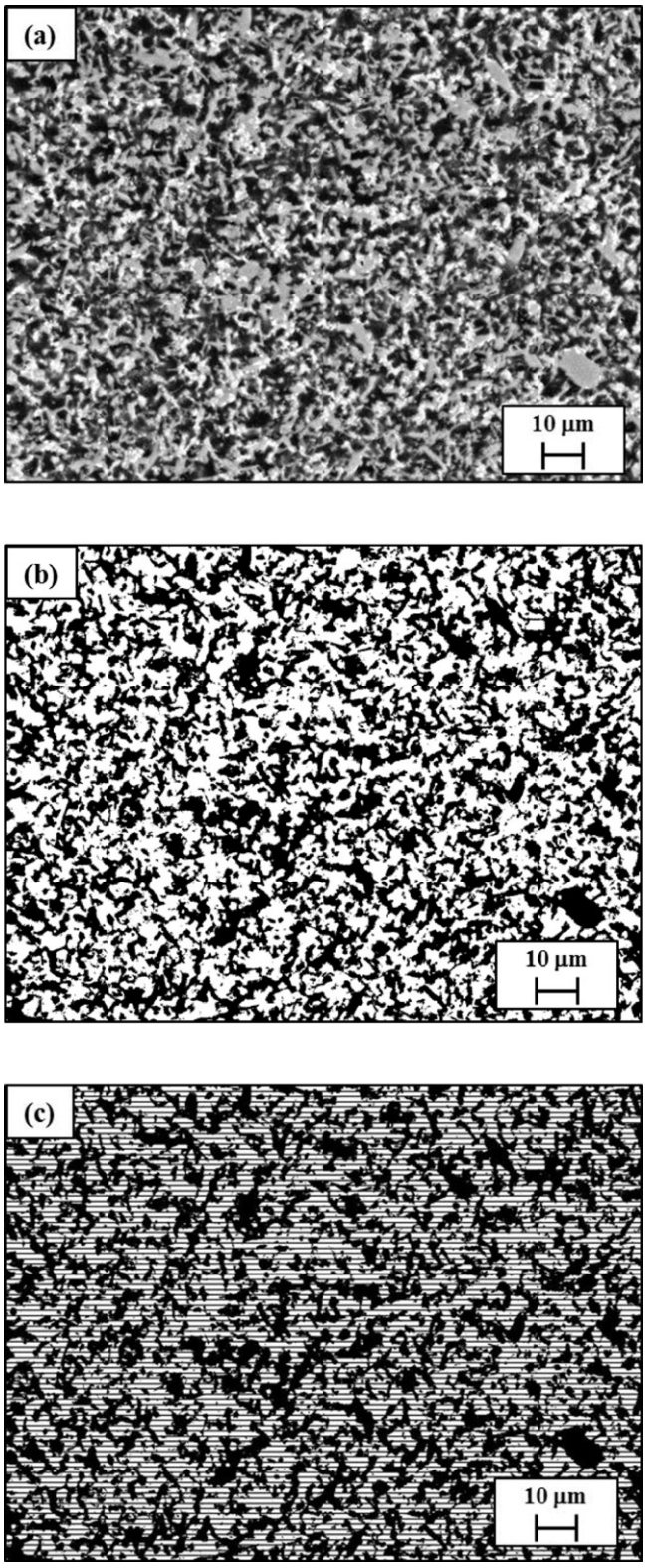

Fig. 8. (a) Polished SEM image, (b) binary image and (c) processed image of AC.

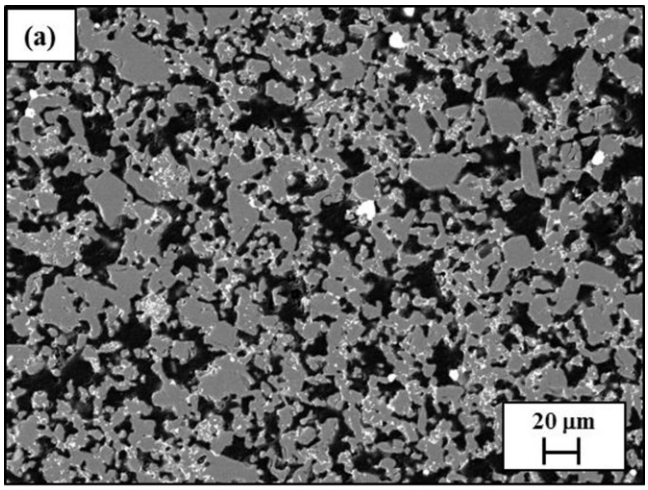

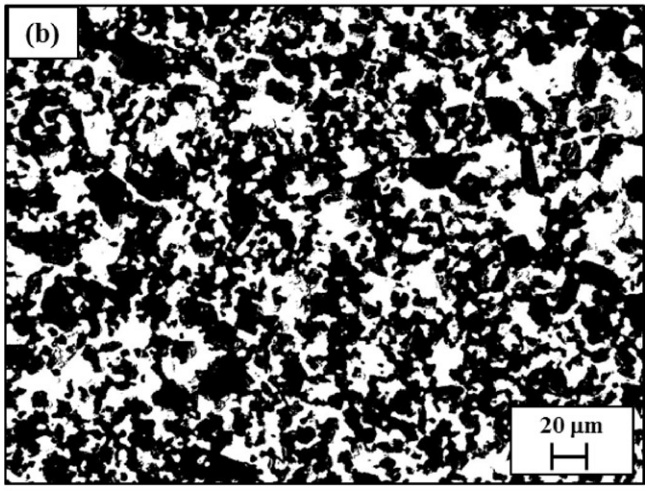

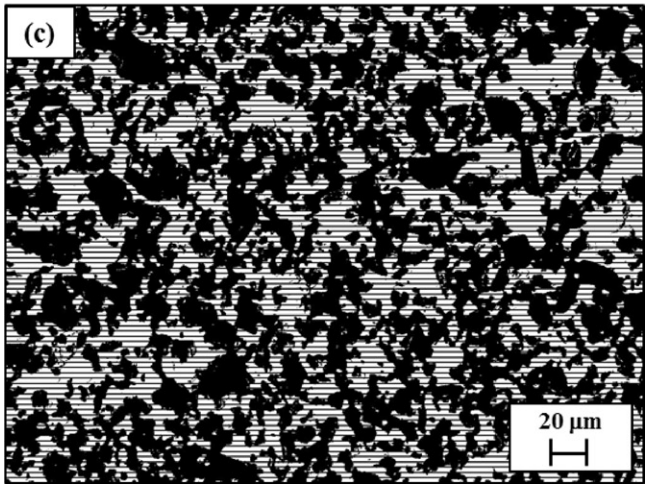

Fig. 9. (a) Polished SEM image, (b) binary image and (c) processed image of BC.

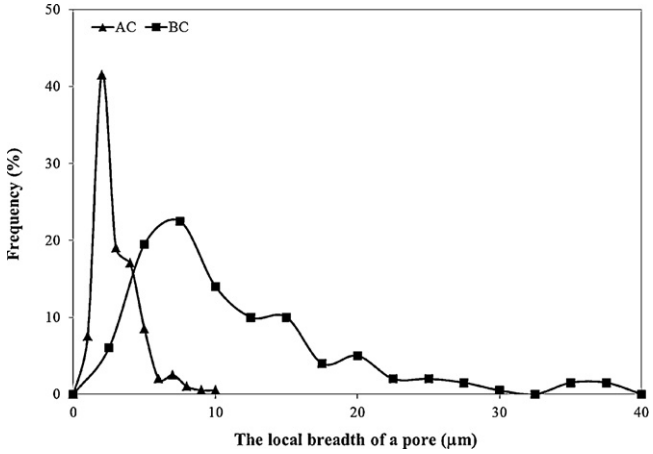

Fig. 10. The local breadth of a pore distribution of AC and BC.

Complex path as a result of interlocking structure of AC restricted drawing continuous lines along the pores that was accepted as local breadth of a pore. This referred the maximum distance where air can flow without meeting any obstacle. Shorter lines were superimposed for AC than for BC (from Figs. 8c and 9c) and smaller local breadth was obtained as plotted in Fig. 10.

Distribution of the local breadth of a pore was given in Fig. 10. While AC has narrow distribution with smaller values, a large distribution with larger length was obtained for BC. The average length of mean free path of AC was 2 μm and of BC was 10 μm.

The random distribution of anisotropic fine β-grains limited the maximum local breadth of AC which was around 7 μm. It has a narrow distribution. On the contrary, isotropic and coarse β-grains produced larger path, hence larger distribution was obtained with a maximum value that was over 35 μm.

4. Conclusions

It is possible to improve the permeability of porous Si_3N_4 by tailoring microstructure. β-Si_3N_4 grains with low aspect ratio formed larger pore channels and regular path for air flow and these changes improved the permeability by several orders of magnitude even though the denser structure of series BC with respect to AC.

Ergun equation could be used for prediction of Darcian permeability, on the other hand it led some errors for non-Darcian permeability. Forchheimer number and the local breadth of a pore also proved the effect of structure on permeability. In spite of the increment in permeability, its value is still lower for practical applications such as diesel particulate filter (DPF) substrates where Darcian permeability should be 10^{-12} m^2.[36]

Acknowledgements

This project has been supported by the Foundation for Scientific Research Projects of Anadolu University (Project number: 090229).

Author G. Topates would like to thank The Scientific and Technological Research Council of Turkey for supporting studies carried out at Fraunhofer IKTS.

References

1. Kawai C, Matsuura T, Yamakawa A. Separation–permeation performance of porous Si_3N_4 ceramics composed of columnar β-Si_3N_4 grains as membrane filters for microfiltration. *J Mater Sci* 1999;**34**:893–6.
2. Antsiferov VN, Gilev VG. Ceramic membranes from reaction-sintered silicon nitride on nitride and oxide substrates. *Refract Ind Ceram* 1998;**39**(11/12):440–3.
3. She J, Yang JF, Beppu Y, Ohji T. Hertzian contact damage in a highly porous silicon nitride ceramic. *J Eur Ceram Soc* 2003;**23**:1193–7.
4. Cheng F, Clark S, Kelly SM, Bradley JS, Lefebvre F. Preparation of mesoporous silicon nitride via a nonaqueous sol–gel route. *J Am Ceram Soc* 2004;**87**(8):1413–7.
5. Park DS, Lee MW, Kim HD, Park YJ, Jung YG. Fabrication and properties of porous RBSN. *Key Eng Mater* 2005;**287**:277–81.
6. Yang J, Yang JF, Shan SY, Gao JQ, Ohji T. Effect of sintering additives on microstructure and mechanical properties of porous silicon nitride ceramics. *J Am Ceram Soc* 2006;**89**(12):3843–5.
7. Hayashi I, Shinohara N, Watanabe T, Takahashi H. Porous silicon nitride for low pressure loss DPF. Reports Res Lab Asahi Glass Co. Ltd. 2006; 56: 25–7.
8. Hoffmann MJ, Petzow G. Tailored microstructures of silicon nitride ceramics. *Pure Appl Chem* 1994;**66**(9):1807–14.
9. Kawai C, Yamakawa A. Effect of porosity and microstructure on the strength of Si_3N_4: designed microstructure for high strength, high thermal shock resistance, and facile machining. *J Am Ceram Soc* 1997;**80**(10):2705–8.
10. Inagaki Y, Kondo N, Ohji T. High performance porous silicon nitrides. *J Eur Ceram Soc* 2002;**22**(14/15):2489–94.
11. Yang J-F, Deng Z-Y, Ohji T. Fabrication and characterisation of porous silicon nitride ceramics using Yb_2O_3 as sintering additive. *J Eur Ceram Soc* 2003;**23**:371–8.
12. Yang J-F, Zhang G-J, Ohji T. Fabrication of low-shrinkage, porous silicon nitride ceramics by addition of a small amount of carbon. *J Am Ceram Soc* 2001;**84**(7):1639–41.
13. Diaz A, Hampshire S, Yang J-F, Ohji T, Kanzaki S. Comparison of mechanical properties of silicon nitrides with controlled porosities produced by different fabrication routes. *J Am Ceram Soc* 2005;**88**(3):698–706.
14. Park Y-J, Park B-W, Lee S-H, Lee J-W, Yun H-S, Saong I-H. The characterization of porous sintered reaction-bonded silicon nitride ceramics fabricated by Si-additive mixture granules. *Int J Appl Ceram Technol* 2011;**8**(6):1501–8.
15. Okano H, Yamaguchi H, Shigenobu R, Obuchi A, Uchisawa J, Porous silicon nitride ceramics with high performance for diesel exhaust after-treatment system. SAE International, 2012-01-0849.
16. Park YJ, Song IH. Si_3N_4 with comparable permeability to SiC. *J Eur Ceram Soc* 2012;**32**:471–5.
17. Moreira EA, Innocentini MDM, Coury JR. Permeability of ceramic foams to compressible and incompressible flow. *J Eur Ceram Soc* 2004;**24**:3209–18.
18. Park YJ, Kim HD, Halloran JW. Permeability enhancement in porous-sintered reaction-bonded silicon nitrides. *Int J Appl Ceram Technol* 2011;**8**(4):809–14.
19. Innocentini MDM, Sepulveda P, Ortega FS. Permeability. In: Scheffler M, Colombo P, editors. *Cellular ceramics*. Weinheim: Wiley VCH Verlag GmbH & Co. KGaA; 2005. p. 313–41.
20. Bird RB, Stewart WE, Lightfood EN. *Transport phenomena*. USA: John Wiley & Sons; 2002. p. 159–98.
21. Lage JL, De Lemos MJS, Nield DD. Modelling turbulence in porous media. In: Ingham DB, Pop I, editors. *Transport phenomena in porous media II*. England: Pergamon Press; 2002. p. 198–202.
22. Janna WS. Internal incompressible viscous flow. In: Richard W. Johnson, editor. *The handbook of fluid dynamics*. USA: CRC Press; 1998. p. 62–3.
23. Ziel R, Haus A, Tulke A. Quantification of the pore size distribution (porosity profiles) in microfiltration membranes by SEM, TEM and computer image analysis. *J Membr Sci* 2008;**323**:241–6.
24. Philipse AP, Schram HL. Non-Darcian airflow through ceramic foams. *J Am Ceram Soc* 1991;**74**(4):728–32.
25. Biasetto L, Colombo P, Innocentini MDM, Mullens S. Gas permeability of microcellular ceramic foams. *Ind Eng Chem Res* 2007;**46**:3366–72.
26. Innocentini MDM, Salvini VR, Macedo A, Pandolfelli VC. Prediction of ceramics foam permeability using Ergun's equation. *Mater Res* 1999;**2**(4):283–9.
27. Ma H, Ruth DW. The microscopic analysis of high Forchheimer number in porous media. *Transport Porous Med* 1993;**13**:139–60.
28. Perera DS, Mitchell DRG, Leung S. High aspect ratio β-Si_3N_4 grain growth. *J Eur Ceram Soc* 2000;**20**:789–94.
29. Matovic B. Low temperature sintering additives for silicon nitride. Dissertation, Stutgart University 2003.
30. Mitomo M, Tsutsumi M, Tanaka H. Grain growth during gas-pressure sintering of β-silicon nitride. *J Am Ceram Soc* 1991;**73**(8):2441–5.
31. Lange FF. Fracture thoughness of Si_3N_4 as a function of the initial α-phase content. *J Am Ceram Soc* 1979;**62**(7/8):428–30.
32. Okamoto Y, Hirosaki N, Akimune Y, Mitomo M. Influence of α to β phase transformation on grain growth rate of silicon nitride. *J Ceram Soc Jpn* 1997;**105**:476–8.
33. Krämer M, Hoffmann MJ, Petzow G. Grain growth studies of silicon nitride dispersed in an oxynitride glass. *J Am Ceram Soc* 1993;**76**(11): 2778–84.
34. Krämer M, Hoffmann MJ, Petzow G. Grain growth kinetics of Si_3N_4 during α/β-transformation. *Acta Metall Mater* 1993;**41**(10):2939–47.
35. Fangli Y, Huanrui W, Yu B, Jianfeng Y. Preparation and characterization of porous Si_3N_4 ceramics prepared by compression molding and slip casting methods. *Bull Mater Sci* 2010;**33**(5):619–24.
36. Adler J. Ceramic diesel particulate filters. *Int J Appl Ceram Technol* 2005;**2**(6):429–39.

Gulsum Topates has worked as a research assistant at Anadolu University, Department of Materials Science and Engineering. She studied ceramic engineering at Anadolu University and received BSc in 2000 and MSc in 2003. She is studying her PhD at the same department. Production and characterization of porous Si_3N_4 based ceramics is the main interest of her.